Sensitivity, Approximation, and Uncertainty in Power System Dynamic Simulation

Ian A. Hiskens, *Fellow, IEEE*, and Jassim Alseddiqui, *Student Member, IEEE*

Abstract—**Parameters of power system models, in particular load models, are seldom known exactly, yet dynamic security assessment relies upon simulation of those uncertain models. This paper proposes a computationally feasible approach to assessing the influence of uncertainty in simulations of power system dynamic behavior. It is shown that trajectory sensitivities can be used to generate accurate first-order approximations of trajectories that arise from perturbed parameter sets. The computational cost of obtaining the sensitivities and perturbed trajectories is minimal. The mathematical structure of the trajectory approximations allows the effects of uncertainty to be quantified and visualized using worst-case analysis and probabilistic approaches.**

Index Terms—**Load modeling, parameter uncertainty, power system dynamic performance assessment, power system simulation, trajectory sensitivity.**

I. INTRODUCTION

DYNAMIC performance assessment underpins the design and operation of power systems. Postulated system conditions and disturbance scenarios are investigated to ensure adequate system behavior. Stability should be maintained, control loops tuned to provide appropriate damping, and safety thresholds such as over/under-voltage limits enforced. Unfortunately, when actual system events occur, post-mortem analysis invariably reveals discrepancies between modeled and measured system behavior. The conclusion is simple: models used for analysis contain erroneous parameters. Resolution of this predicament is, however, far from straightforward.

All parameter values are uncertain to some extent. Measurement and model validation [1]–[3] plays an important role in reducing that uncertainty, particularly for well-defined components such as generators and network elements. However, load models provide a conundrum. It is impractical to represent every load within a large power system. Generally, models are a composite representation of many small, diverse loads.[1] This loss of fidelity introduces uncertainty into load model behavior. Furthermore, load composition is continually changing to match consumer requirements. Therefore, even if a load model could be accurately identified at a certain time, it would likely be inaccurate at any other time.

A similar argument holds for distributed generation. As the penetration of smaller distributed resources increases, so will their effects on overall system dynamic behavior. However, it is impractical to model every source, so aggregation is again necessary, and uncertainty is unavoidable.

Accounting for uncertainty in dynamic performance assessment is computationally challenging. A naïve Monte Carlo approach would require a full time-domain simulation for every randomly generated set of parameters. Clearly, for many uncertain parameters, such an investigation is infeasible. This paper proposes a computationally efficient approach to assessing the impact of parameter uncertainty.

Various approaches to addressing uncertainty in dynamic performance assessment have been proposed. Disturbance and operating point uncertainty are considered in [4] and [5], for example, though parametric uncertainty is not discussed. Parametric uncertainty is addressed in [6], where the probabilistic collocation method is used to develop polynomial relationships between uncertain parameters and quantities (outputs) of interest. This ingenious technique is computationally efficient when the number of uncertain parameters is relatively small. Another novel approach, developed in the context of power electronics, uses polynomial chaos theory [7] to assess the effects of parameter uncertainty. A discussion of a trajectory sensitivity-based approach to approximating the effects of parameter uncertainty was presented in [8]. Those preliminary results are extended in this present paper.

Sensitivity concepts are generally associated with the linearization of an input-output relationship. Small changes in inputs map through the linearized relationship to small output changes.[2] Trajectory sensitivities fit this framework by describing the changes in the trajectory (the output) resulting from perturbations in the underlying parameters and/or initial conditions (the inputs). They provide a linearization around the trajectory, as against small disturbance analysis, which builds on linearization around the equilibrium point. Full details are provided in Section III. Trajectory sensitivity concepts are not new [9]–[11], though until recently, progress on practical applications was impeded by the following.

- *Computational inefficiency.* Sensitivity to each parameter or initial condition required an additional full simulation.
- *Nonsmooth behavior.* Sensitivities were not well defined for situations where events influenced behavior.

---

[1]Certain loads, though, such as aluminium smelters, are well defined.

[2]Consider, for example, power flow sensitivity, where the inverse Jacobian maps power perturbations to voltage changes.

However, both these limitations have recently been overcome, with efficient computation of trajectory sensitivities now possible for large-scale, nonsmooth systems [12], [13]. Further details are provided later.

As mentioned previously, load modeling is a major source of uncertainty in power system dynamic performance assessment. A number of the illustrations throughout this paper will therefore focus on load modeling. It is common for aggregate load models to be composed of a static voltage-dependent component together with an induction motor [14], [15]. This composition can be described parametrically by

$$S_{tot} = \nu S_v + (1 - \nu)S_{ind} \tag{1}$$

where S_{tot} is the total complex power of the load

$$S_v = P_0 V^{\eta_p} + jQ_0 V^{\eta_q} \tag{2}$$

describes the voltage-dependent part of the load, and S_{ind} is the complex power demanded by the induction motor component. The dynamics underlying S_{ind} are typically described by a third-order differential equation model [16]. Each of the load components in (1) should be sized to match the total bus demand. The parameter ν provides the necessary scaling, with 100ν specifying the percentage of static load. The distribution of load between S_v and S_{ind}, i.e., the value of ν, can have a nontrivial effect on system dynamic performance. Often, though, this distribution is imprecisely known. Later examples will consider uncertainty in η_p, η_q, and ν.

Disturbances that cascade beyond local events generally do so as a consequence of unexpected protection operation. The initial (designed) protection response leaves the system in a weakened state, vulnerable to subsequent unanticipated protection operation. These secondary protection trips are often not foreseen because

1) investigations of dynamic performance focus on questions of stability/instability, with protection devices not even monitored, or
2) the nominal trajectory is well behaved with respect to protection, even though plausible combinations of uncertain parameters induce unacceptable behavior.

This paper provides an example of the latter situation, where consideration of load parameter uncertainty suggests exposure to distance protection operation.

This paper is structured as follows. Section II describes a model that is structured to capture the full range of nonlinear nonsmooth behavior exhibited by power systems. An overview of trajectory sensitivities is provided in Section III. Those sensitivities are used in Section IV to generate trajectory approximations. It is shown in Section V that such approximations form the basis for quantifying and visualizing the influence of parameter uncertainty. Conclusions are provided in Section VI.

II. MODEL

In response to large disturbances, power systems typically exhibit periods of smooth behavior, interspersed with discrete events. Smooth behavior is driven by devices such as generators,

which are well described analytically by differential-algebraic models. Discrete events, arising, for example, from operation of protection devices or enforcement of controller hard limits, are not so easy to describe analytically. Systems that exhibit intrinsic interactions between continuous dynamics and discrete events have become known generically as *hybrid systems* [17], [18] or *piecewise smooth dynamical systems* [19].

Numerous formal models, such as Petri nets [20] and hybrid automata [17], exist for rigorously describing hybrid system dynamics. However, those representations are not immediately amenable to numerical implementation. Analysis of power system dynamics requires a nonrestrictive model formulation that is capable of capturing the full range of continuous/discrete hybrid system dynamics yet is computationally efficient. It is shown in [13] and [21] that these specifications are met by a model that consists of a set of differential-algebraic equations, adapted to incorporate switching of the algebraic equations, and impulsive (state reset) action. This DA *Impulsive Switched* (DAIS) model has its genesis in the familiar DAE model

$$\dot{x} = f(x, y) \tag{3}$$
$$0 = g(x, y) \tag{4}$$

where $x \in \mathbb{R}^n$ are dynamic states, $y \in \mathbb{R}^m$ are algebraic states, $f : \mathbb{R}^{n+m} \to \mathbb{R}^n$, and $g : \mathbb{R}^{n+m} \to \mathbb{R}^m$.

Switching events, such as line tripping, can be incorporated into the DAE model by requiring the algebraic equations (4) to switch between sets of equations that describe pre- and post-event conditions. Considering a single switching event, (4) can be replaced by

$$0 = g(x, y) \triangleq \begin{cases} g^-(x, y), & s(x, y) < 0 \\ g^+(x, y), & s(x, y) > 0 \end{cases} \tag{5}$$

where the superscripts "−" and "+" index the two sets of algebraic equations.[3] A switching event coincides with a zero crossing of the trigger function $s(x, y)$. Note that the concept of crossing is important. If the trajectory just touches (grazes) the triggering surface

$$\mathcal{S} = \{(x, y) : s(x, y) = 0\} \tag{6}$$

then behavior beyond that point is indeterminent, as switching may or may not occur [22]. Therefore, the following assumption is required.

Assumption 1: The trajectory encounters the triggering surface $\mathcal{S}$ transversally.

The precise behavior of the model at a switching event is not well defined by (5) and requires further explanation. Let the event occur at trigger time τ, and define τ^- as the time instant just prior to τ and τ^+ as the instant just after τ. The limit values of the states can then be expressed as

$$x^- \equiv x(\tau^-) := \lim_{t \uparrow \tau} x(t), \qquad x^+ \equiv x(\tau^+) := \lim_{t \downarrow \tau} x(t) \tag{7}$$

$$y^- \equiv y(\tau^-) := \lim_{t \uparrow \tau} y(t), \qquad y^+ \equiv y(\tau^+) := \lim_{t \downarrow \tau} y(t) \tag{8}$$

---

[3]The functions g^- and g^+ may themselves have a switched form, resulting in a hierarchical switching structure.

where $t \uparrow \tau$ implies $t < \tau$ approaches τ from below, and $t \downarrow \tau$ implies $t > \tau$ approaches τ from above. Clearly, two sets of variables (x^-, y^-) and (x^+, y^+) are required to fully describe behavior at an event [23].

By definition, $s(x^-, y^-) = 0$, but $s(x^+, y^+)$ may not necessarily equal zero. Furthermore, assume without loss of generality that $s(x(t), y(t)) < 0$ for $t < \tau$. Then well-defined switching behavior requires $s(x(t), y(t)) > 0$ for $t > \tau$. Also, this sign assumption implies $g^-(x^-, y^-) = 0$ and $g^+(x^+, y^+) = 0$. Dynamic states are unaltered at a switching event, so $x^- = x^+$. However, in order to satisfy the altered algebraic equations, often, $y^- \neq y^+$.

Switching events cannot efficiently capture all forms of discrete behavior. Activities such as transformer tapping or protection timer resetting [24] are best modeled by impulsive action that introduces discrete jumps into the dynamic x-states. Such behavior has the form of an impulse, which can be described by a reset equation

$$x^+ = h(x^-, y^-), \quad \text{when } s(x, y) = 0 \qquad (9)$$

where $h : \mathbb{R}^{n+m} \to \mathbb{R}^n$. The superscript notation is consistent with earlier use, with x^+ denoting the value of x just after the reset event, while x^- and y^- refer to the values of x and y just prior to the event. As in the case of a switching event, a reset event is triggered when $s(x, y)$ passes through zero. Away from that zero crossing condition, the evolution of the dynamic x-states is described by the differential equations (3).

This overview of the DAIS model has neglected some of the technical details required to ensure well-defined behavior. However, full details are provided in [21]. It should be emphasized that the DAIS model is nothing more than a formalization of simulation models that are used for practical power system simulation. The formalization, however, allows trajectory sensitivities to be cleanly defined [13].

Dynamic behavior, generated numerically by simulation, can be described analytically by the *flow*

$$x(t) = \phi(x_0, t) \qquad (10)$$
$$y(t) = \psi(x_0, t). \qquad (11)$$

Initial conditions imply

$$\phi(x_0, t_0) = x_0 \qquad (12)$$
$$g(\phi(x_0, t_0), \psi(x_0, t_0)) = 0. \qquad (13)$$

A compact development of trajectory sensitivities results from incorporating parameters $p \in \mathbb{R}^\ell$ into the dynamic states x. (Numerical implementation is also simplified.) This is achieved by introducing trivial differential equations

$$\dot{p} = 0 \qquad (14)$$

into (3) and results in the natural partitioning

$$x = \begin{bmatrix} x \\ p \end{bmatrix}, \qquad f = \begin{bmatrix} f \\ 0 \end{bmatrix}, \qquad h = \begin{bmatrix} h \\ p \end{bmatrix} \qquad (15)$$

where $\underline{x}$ are the true dynamic states, and p are parameters. Accordingly, initial conditions and parameters will be treated synonymously throughout the remainder of this paper.

III. TRAJECTORY SENSITIVITY

A. Motivation

The functional form of the flow (10)–(11) motivates the Taylor series expansions

$$\phi(x_0 + \Delta x_0, t) = \phi(x_0, t) + \frac{\partial \phi(x_0, t)}{\partial x_0} \Delta x_0 + \mathcal{E}^\phi(x_0, t, \Delta x_0) \qquad (16)$$

$$\psi(x_0 + \Delta x_0, t) = \psi(x_0, t) + \frac{\partial \psi(x_0, t)}{\partial x_0} \Delta x_0 + \mathcal{E}^\psi(x_0, t, \Delta x_0) \qquad (17)$$

where $\mathcal{E}^\phi$ and $\mathcal{E}^\psi$ capture the higher order terms. For small $\|\Delta x_0\|$, the higher order terms may be neglected, giving

$$\Delta x(t) = \phi(x_0 + \Delta x_0, t) - \phi(x_0, t)$$
$$\approx \frac{\partial \phi(x_0, t)}{\partial x_0} \Delta x_0 \equiv \Phi(x_0, t) \Delta x_0 \qquad (18)$$
$$\Delta y(t) = \psi(x_0 + \Delta x_0, t) - \psi(x_0, t)$$
$$\approx \frac{\partial \psi(x_0, t)}{\partial x_0} \Delta x_0 \equiv \Psi(x_0, t) \Delta x_0 \qquad (19)$$

where Φ and Ψ are the *sensitivity transition matrices*, or *trajectory sensitivities*, associated with the x and y flows [11]. Equation (18) describes the approximate change $\Delta x(t)$ in a trajectory, at time t along the trajectory, for a given small[4] change in initial conditions $\Delta x_0 = [\Delta \underline{x}_0^T \ \Delta p^T]^T$. Likewise, the change $\Delta y(t)$ is given by (19).

B. Variational Equations

The evolution of the trajectory sensitivities Φ and Ψ is described by variational equations[5] that are developed in [13]. Aspects of these equations are required for the later discussion of trajectory approximations, so the following summary draws together the main concepts.

Away from events, where system dynamics evolve smoothly, the sensitivities Φ and Ψ are obtained by differentiating (3)–(4) with respect to x_0. This gives

$$\dot{\Phi} = f_x(t)\Phi + f_y(t)\Psi \qquad (20)$$
$$0 = g_x(t)\Phi + g_y(t)\Psi \qquad (21)$$

where $f_x \equiv \partial f / \partial x$, and likewise for the other Jacobian matrices. Note that f_x, f_y, g_x, and g_y are evaluated along the trajectory and hence are time-varying matrices. The computational burden of numerically integrating this (potentially high order) linear time-varying DAE system, though, is minimal. It is shown in [12], [13], and [27] that when an implicit numerical integration technique such as trapezoidal integration is used, the solution of (20)–(21) can be obtained as a by-product of computing the underlying trajectory.

[4]It is very difficult to quantify acceptable perturbation size. This issue is explored further in Sections IV-A and IV-B.

[5]These variational equations relate quite closely to the application of calculus of variations concepts [25] to optimal control problems [26].

Initial conditions for Φ are obtained from (12) as

$$\Phi(x_0, t_0) = I \tag{22}$$

where I is the identity matrix. Initial conditions for Ψ follow directly from (21)

$$0 = g_x(t_0) + g_y(t_0)\Psi(x_0, t_0). \tag{23}$$

Equations (20)–(21) describe the evolution of the sensitivities Φ and Ψ between events. However, the sensitivities are often discontinuous at events. It is necessary to calculate *jump conditions* describing event-induced step changes in Φ and Ψ. Consider the most general case of a coincident switching/reset event, described by (5) and (9). (The jump conditions appropriate for separate switching or reset events follow directly from this more general situation.) It is shown in [13] that the jump conditions for the sensitivities Φ are given by

$$\Phi(x_0, \tau^+) = h_x^* \Phi(x_0, \tau^-) - \left(f^+ - h_x^* f^-\right) \tau_{x_0} \tag{24}$$

where

$$\tau_{x_0} \equiv \frac{\partial \tau}{\partial x_0} = -\frac{s_x^* \Phi(x_0, \tau^-)}{s_x^* f^-} \tag{25}$$

and

$$f^- \equiv f(x^-, y^-) \tag{26}$$
$$f^+ \equiv f(x^+, y^+) \tag{27}$$
$$h_x^* = \left. \left(h_x - h_y g_y^{-1} g_x\right)\right|_{\tau^-} \tag{28}$$
$$s_x^* = \left. \left(s_x - s_y g_y^{-1} g_x\right)\right|_{\tau^-}. \tag{29}$$

Note that jump conditions are only well defined when Assumption 1 is satisfied. Otherwise, if the trajectory encounters $\mathcal{S}$ tangentially rather than transversally, the denominator of (25) will equal zero. The sensitivities Ψ immediately after the event are given by

$$\Psi(x_0, \tau^+) = - \left. \left(g_y^{-1} g_x\right)\right|_{\tau^+} \Phi(x_0, \tau^+). \tag{30}$$

Keep in mind that g in (28)–(29) refers to its pre-event form, whereas post-event conditions apply in (30).

Subsequent to the event, for $t > \tau^+$, calculation of the sensitivities proceeds according to (20)–(21). The jump conditions (24) and (30) provide the initial conditions for this post-event integration.

C. Example—Parameter Ranking

Trajectory sensitivities provide a basis for ranking the relative influence of parameters. Large sensitivities imply that parameter variations have a large effect on behavior, whereas small sensitivities suggest behavior changes very little with parameter variation. In this example, trajectory sensitivities are used to rank the importance of voltage indexes at all loads throughout the IEEE 39-bus system of Fig. 1.
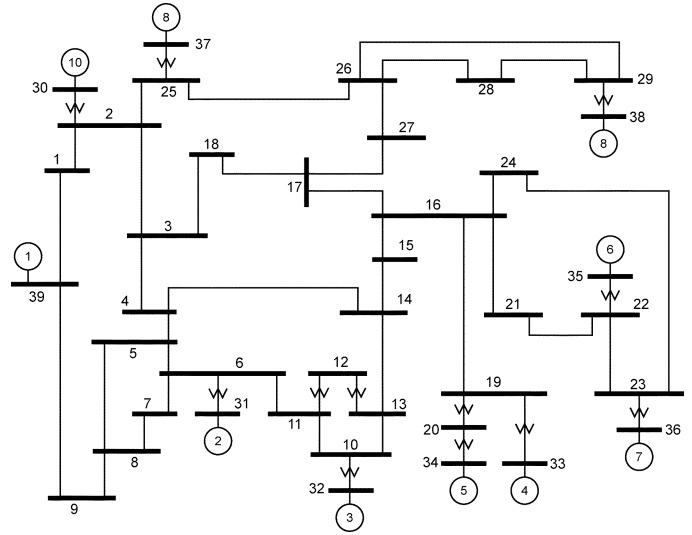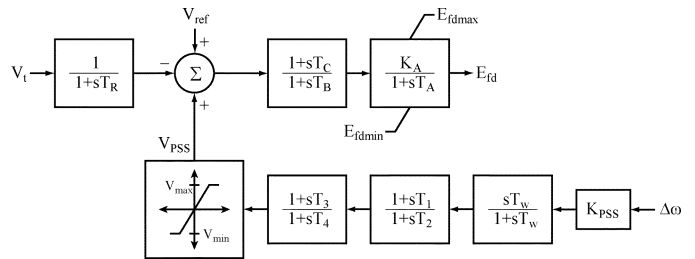

Fig. 1. IEEE 39-bus system.

Fig. 2. AVR/PSS standard models AC4A and PSS1A.

All generators in this system were represented by a fourth-order machine model [28] and were regulated by the IEEE standard [29] AVR/PSS representation of Fig. 2. All generator and network data were obtained from [30]. A three-phase fault was applied at bus 16 at 0.1 s and cleared (without any line tripping) 0.2 s later. The static load model (2) was used for all loads, with $\eta_p = \eta_q = 2$ in all cases.

The sensitivities of bus 16 voltage V_{16} to load indexes η_p and η_q at all buses were computed in conjunction with the nominal trajectory. These trajectory sensitivities are provided in Fig. 3, where the vertical axis gives the change in the per unit voltage for a unity change in load index values. It is immediately clear that the real power index η_p for bus 20 has a much greater influence on behavior than all other indexes. (The reason is that generator 5 is marginally stable for this disturbance scenario, and bus 20 lies on the corridor linking that generator to the rest of the system.) The loads at buses 4, 8, and 23 also display a reasonable, though certainly less pronounced, level of influence. Loads 4 and 8 are influential due to their large size. Load 23 has an important impact on the dynamics of generator 7. The influence of all other loads, for this disturbance scenario, is negligible. Of course, a different disturbance could possibly highlight some other set of loads.

Field testing loads to determine their (approximate) voltage dependence is an expensive exercise. However, by utilizing tra-
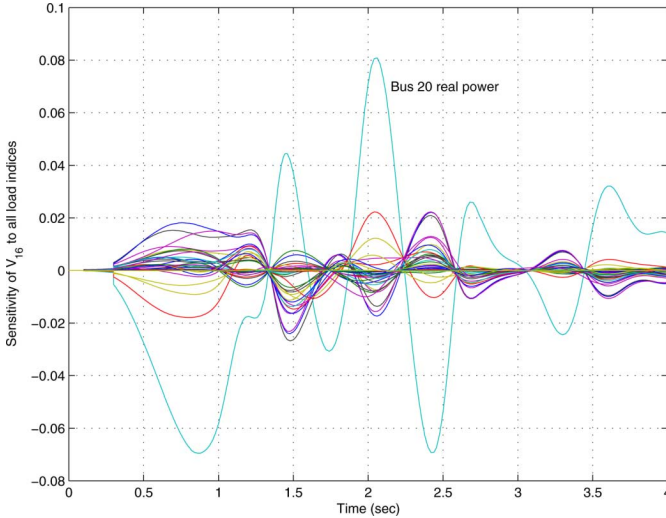
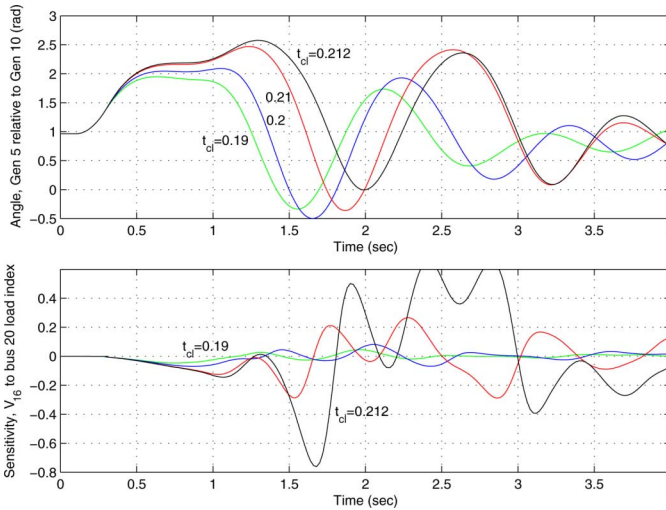Fig. 3.   Trajectory sensitivities for all load indexes.

Fig. 4.   Trajectory and sensitivity variation for increasing system stress.

jectory sensitivities, the most important loads can be identified and attention focused accordingly. This use of trajectory sensitivities relates to parameter identifiability and was used in [3] to determine the most influential generator parameters.

D. Example—Indicator of Stressed Conditions

As systems become more heavily stressed, their sensitivity to parameter variation increases significantly. This can be illustrated by continuing the example from Section III-C. The upper plot of Fig. 4 shows the behavior of generator 5 angle (relative to generator 10) for a range of fault clearing times. (For comparison, the fault clearing time used in Section III-C was 0.2 s.) The critical clearing time is 0.213 s; slower clearing results in generator 5 losing synchronism. Notice that the angular deviations do not show a great increase, even though instability is imminent.

The sensitivity of V_{16} to the bus 20 load index η_p, for the same range of fault clearing times, is shown in the lower plot of Fig. 4. The deviations exhibited by these trajectory sensitivities

grow dramatically as critical conditions are approached. This behavior motivated the sensitivity-related measures developed in [31] and [32] to predict conditions that induce marginal stability. Further work is required, though, to fully exploit this phenomenon.

IV.   Trajectory Approximation

A. General Concepts

For general nonlinear systems, the flow functions ϕ and ψ, given by (10)–(11), cannot be expressed in closed form. Any change in initial conditions[6] therefore requires a complete re-simulation of the dynamic model. However, if changes are relatively small, the computational effort of repeated simulation can be avoided by forming approximate trajectories.

Rearranging (18)–(19) gives the first-order approximations of the flow

$$\phi(x_0 + \Delta x_0, t) \approx \phi(x_0, t) + \Phi(x_0, t)\Delta x_0 \qquad (31)$$

$$\psi(x_0 + \Delta x_0, t) \approx \psi(x_0, t) + \Psi(x_0, t)\Delta x_0. \qquad (32)$$

As mentioned previously, the trajectory sensitivities Φ and Ψ can be computed efficiently as a by-product of simulating the nominal trajectory. Therefore, a range of (approximate) perturbed trajectories are available via (31)–(32) for the computational cost of a single nominal trajectory. This computational efficiency will be exploited in Section V to explore the influence of parameter uncertainty.

The errors in the approximations (31)–(32) are given by the higher order terms $\mathcal{E}^\phi$ and $\mathcal{E}^\psi$ of the Taylor series. In general, the precise forms of these terms are not available. (If they were, the flow could be expressed in closed form, and repeated simulation would be unnecessary.) It can be easily shown, though, that for linear systems, the error terms vanish, i.e., the approximations are exact. It may be concluded that the error terms will be small for systems that exhibit near-linear behavior, especially when the perturbations $\|\Delta x_0\|$ are small.

Even though power systems are nonlinear, operation close to the stable equilibrium point is nearly linear. The following example explores the interplay between proximity to the equilibrium point, near-linearity, perturbation size, and error magnitude. Errors in the approximate trajectories will be normalized according to

$$err(x_0, \Delta x_0) = \max_i \left\{ \frac{\|\mathcal{E}_i^\phi(x_0, t, \Delta x_0)\|_\infty}{\|\phi_i(x_0, t)\|_\infty} \right\} \qquad (33)$$

which utilizes the supremum norm

$$\|\xi(t)\|_\infty = \max_{t_0 \le t \le t_f} |\xi(t)| \qquad (34)$$

for scalar function $\xi(\cdot)$. Referring to (16), the numerator of (33) gives the norm of the higher order terms (the error) for each state i. It is obtained (numerically) by simulating the true perturbed

[6]Keep in mind that parameters are incorporated into the initial conditions.
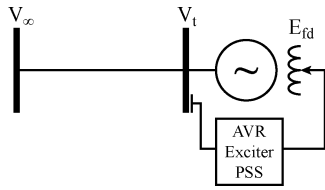
Fig. 5. Single-machine infinite-bus system.

Fig. 6. Error variation with perturbation size.

trajectory and subtracting the corresponding approximate trajectory. The denominator normalizes those errors to allow comparison across different states.

B. Example—Smooth Behavior

The single-machine infinite-bus system of Fig. 5 forms the basis for this illustration of the quality of trajectory approximation achievable by (31)–(32). The generator in this system was represented by a sixth-order machine model [28]. Its AVR/PSS was modeled according to the representation shown in Fig. 2. For this example, the limits on field voltage and PSS output were disabled, to ensure smooth behavior. The influence of limits is considered in subsequent sections.

For this example, the nominal trajectory was not obtained by subjecting the system to an initiating disturbance. Rather, all initial conditions were set to their equilibrium values, except for the generator frequency state ω. Various initial (non-equilibrium) values of ω will be considered, allowing an investigation of the influence of system stress on the quality of trajectory approximations.

For the first case, the nominal trajectory was obtained by setting ω to an initial value of $\omega(t_0) = -4$ rad/s, with all other states initially at their equilibrium values. Approximate trajectories were then synthesized using (31)–(32) for a range of initial conditions $x_0 + \Delta x_0$, where all elements of Δx_0 were zero except for the $\Delta \omega(t_0)$ element, which took values of $0.5, 1.0, 1.5, \ldots, 6.0$. These approximate trajectories were compared with the corresponding true perturbed trajectories, and the normalized error was computed according to (33). The flattest curve in Fig. 6 shows the results, with the normalized error points shown as circles. These points closely fit a straight line with very small slope. All errors are small in this case, even when perturbations are large. This would suggest the system behaves almost like a linear system, with nonlinearities having very little influence.

The middle curve in Fig. 6 corresponds to the nominal trajectory obtained by setting $\omega(t_0) = +4$ rad/s, with all other states initially at their equilibrium values. The above procedure was repeated, though in this case, approximate trajectories were obtained for $\Delta \omega(t_0)$ taking values of $-0.5, -1.0, -1.5, \ldots, -6.0$. The calculated error points are shown as stars. These points almost exactly fit a quartic polynomial and display much greater curvature than in the previous case. This suggests the nominal trajectory is more strongly influenced by nonlinearities. In fact, that is the case, with this nominal trajectory passing closer to an unstable equilibrium point. This is a very nonlinear effect, as linear systems do not possess multiple equilibria.

The upper curve in Fig. 6 was obtained for a nominal trajectory with $\omega(t_0) = +6$ rad/s and all other states again initially
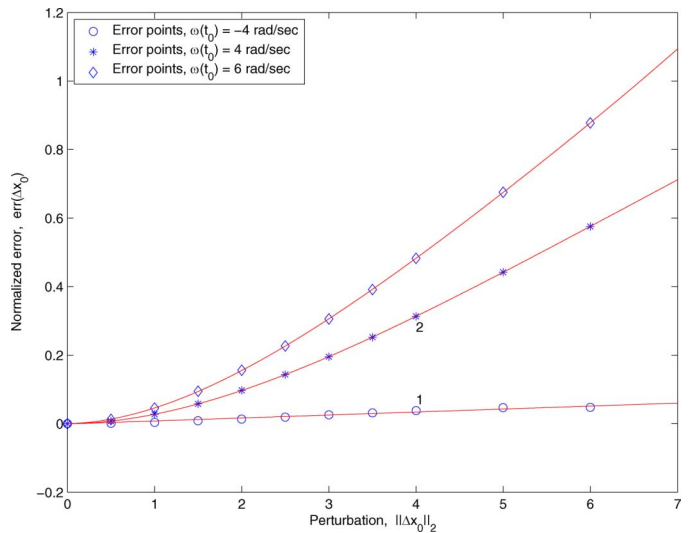
at their equilibrium values. Error points were obtained as before and are shown as diamonds. They again fit a quartic polynomial, though with higher curvature than the previous case. This nominal trajectory passes even closer to the unstable equilibrium point. The higher curvature is consistent with the increased influence of nonlinearities.

Notice that in all three cases, good approximations are obtained, even for relatively large perturbations.

It is insightful to look more closely at the situations underlying the points identified as 1 and 2 in Fig. 6. At point 1, x_0 consists of equilibrium values, except for $\omega(t_0) = -4$, and Δx_0 is all zeros, except for $\Delta \omega(t_0) = 4$. Therefore, $x_0 + \Delta x_0$ describes the equilibrium point, and a trajectory initiated at this point should be constant. Fig. 7 shows the approximate trajectory synthesized for $x_0 + \Delta x_0$ as a dash-dot line. It deviates from zero by only a small amount. Consider the row of (31) corresponding to ω. The left-hand side should be zero, so the sensitivity term on the right should ideally be the negative of the nominal trajectory. Fig. 7 shows that the negated sensitivity term, shown as a dashed line, closely tracks the nominal trajectory, which is the solid line. Though not shown, all other states display similar accuracy.

Likewise for point 2, $\omega(t_0) = 4$, and $\Delta \omega(t_0) = -4$, so $x_0 + \Delta x_0$ again describes equilibrium conditions. Fig. 8 shows the approximated "equilibrium" trajectory as a dash-dot line. In this case, the approximation to equilibrium conditions is not so accurate. However, the negated sensitivity term, shown as a dashed line, does track the nominal trajectory (solid line) quite closely, except for a slight phase shift. That phase shift, though, is sufficient to induce the error apparent in the approximate trajectory.

These latter examples have exploited the special nature of the "equilibrium" trajectories associated with points 1 and 2 of Fig. 6. Subsequent analysis and examples will, however, establish much greater versatility in the use of trajectory approximations.
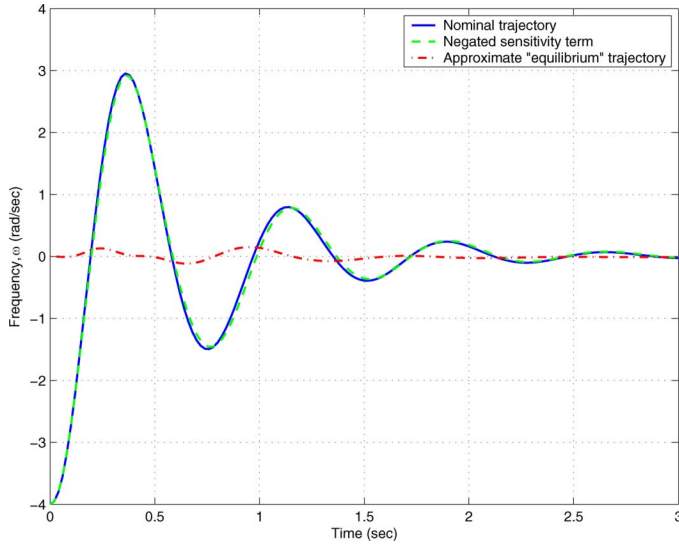
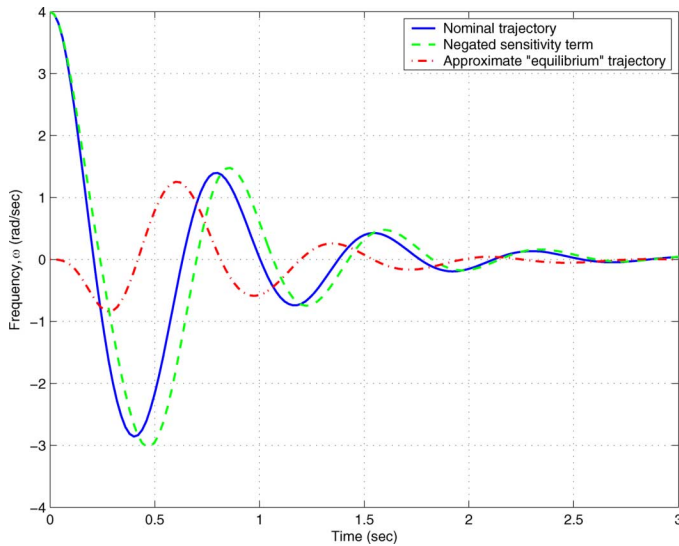Fig. 7. Trajectory approximation, for $\omega(t_0) = -4$ rad/s.

Fig. 8. Trajectory approximation, for $\omega(t_0) = 4$ rad/s.

C. Correction for Event Time Shifts

Variations in initial conditions (including parameters) frequently cause changes in event triggering times. The sensitivity of triggering time to initial conditions is given by τ_{x_0} in (25) and can be interpreted with the assistance of Fig. 9. This figure shows the nominal trajectory, together with a perturbed trajectory induced by a change Δx_0 in initial conditions. The nominal trajectory encounters the triggering hypersurface at time τ, whereas the perturbed trajectory takes an extra time $\Delta \tau = \tau_{x_0} \Delta x_0$ to reach triggering conditions. For clarity, the figure shows positive $\Delta \tau$. However, this time difference could just as easily be negative.

Over the $\Delta \tau$ period, the nominal and perturbed trajectories are driven by different system conditions. In one case, the event has occurred, whereas in the other, it has not. Under such circumstances, the Taylor series expansions (16)–(17) are not valid, so neither are the approximations (31)–(32). A revised process for approximating perturbed behavior over the $\Delta \tau$
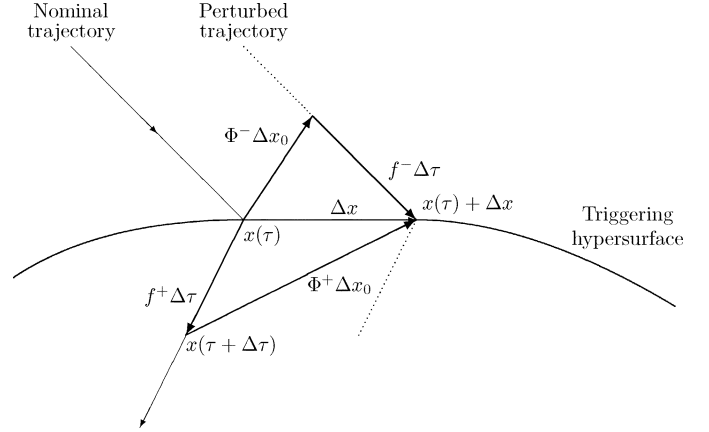

Fig. 9. Linearized view of behavior at an event.

period is presented in [13]. Motivated by the linearized view of event behavior given in Fig. 9, it can be shown that for $\Delta \tau > 0$, approximate trajectories are given by

$$\phi(x_0 + \Delta x_0, t) \approx \phi(x_0, \tau^-) + \Phi(x_0, \tau^-)\Delta x_0 \\ + f^- \times (t - \tau) \tag{35}$$

$$\psi(x_0 + \Delta x_0, t) \approx \psi(x_0, \tau^-) + \Psi(x_0, \tau^-)\Delta x_0 \\ - (g_y^{-1} g_x)\big|_{\tau^-} f^- \times (t - \tau) \tag{36}$$

over the period $\tau \leq t < \tau + \Delta \tau$, where f^- is defined by (26). For $\Delta \tau < 0$, the perturbed trajectory switches before the nominal trajectory. In that case

$$\phi(x_0 + \Delta x_0, t) \approx \phi(x_0, \tau^+) + \Phi(x_0, \tau^+)\Delta x_0 \\ + f^+ \times (t - \tau) \tag{37}$$

$$\psi(x_0 + \Delta x_0, t) \approx \psi(x_0, \tau^+) + \Psi(x_0, \tau^+)\Delta x_0 \\ - (g_y^{-1} g_x)\big|_{\tau^+} f^+ \times (t - \tau) \tag{38}$$

over the period $\tau + \Delta \tau < t \leq \tau$, with f^+ given by (27).

D. Example—Nonsmooth Behavior

This example again uses the system of Fig. 5. In this case, though, the field voltage and PSS limits, shown in Fig. 2, have been reinstated. The system was subjected to a balanced three-phase fault on the generator terminal bus. The fault was cleared without line tripping.

The nominal trajectory, shown in Fig. 10 as a dashed line, was obtained for a fault clearing time of $t_{cl} = 0.23$ s and a maximum field voltage limit of $E_{fd,\max} = 5.8$ pu. Notice that behavior is quite nonsmooth, due to the fault and limit-related events.

Trajectory sensitivities were used to synthesize the approximate behavior that would occur for altered parameter values $t_{cl} = 0.21$ s and $E_{fd,\max} = 5.0$ p.u. (cf. the original values of 0.23 s and 5.8 p.u., respectively.) This synthesized trajectory is shown as the solid line in Fig. 10. For comparison purposes, the full simulation was repeated using these altered parameters. The corresponding trajectory is shown as a dash-dot line in Fig. 10.

The parameters chosen for this illustration exert a significant nonlinear, nonsmooth influence over system behavior. However, even though the change in these parameters is large, the approximated trajectory closely tracks the actual perturbed trajectory. The parameter variations have altered the times at which events
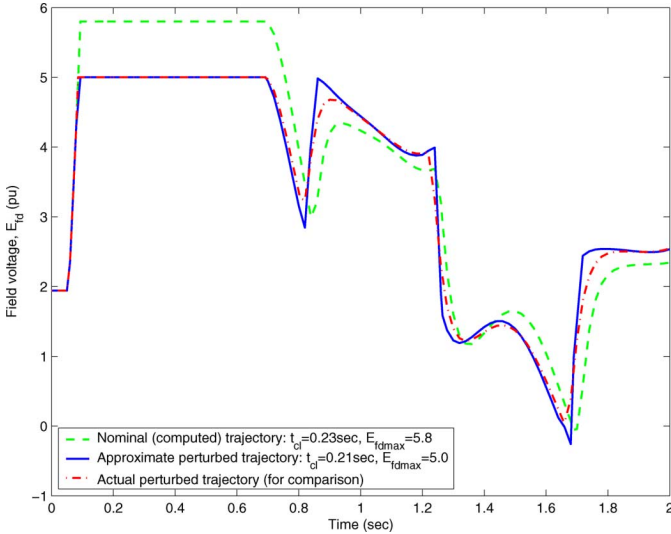
Fig. 10. Field voltage behavior: comparison of actual and approximate trajectories.
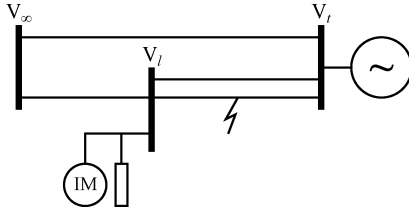

Fig. 11. Three-bus system with composite load.

Fig. 12. Comparison of actual and approximate trajectories for varying load composition.

occur, i.e., when limits are encountered. The approximation is not detrimentally affected though, due to the corrections introduced through (35)–(38).

E. Example—Load Composition

Post-disturbance investigations of power system dynamic performance often reveal situations where load response is inadequately represented by available models. Such studies underlie a perennial desire for improved modeling of load dynamics [15]. However, load composition is often stochastic, suggesting that a single set of parameters cannot capture the full range of expected behavior. Rather, parameters should be specified in terms of their statistical properties. This issue is considered in Section V, through the use of approximate trajectories. For now, trajectory approximations arising from variations in the load composition, governed by ν in the load model (1), will be explored.

The system shown in Fig. 11 will be used to explore the quality of such approximations. The composite load has a steady-state value of $S_{tot} = 40 + j20$ MVA. The static load component was modeled as constant current, while the induction motor component used parameter values from [16, p. 305], with appropriate per unit scaling. Generator production of 250 MW resulted in a fairly stressed system, as suggested by a pre-disturbance angle of $34°$ at the generator terminal bus. Note that the composite load exerts a substantive influence on system dynamics due to its location and size.
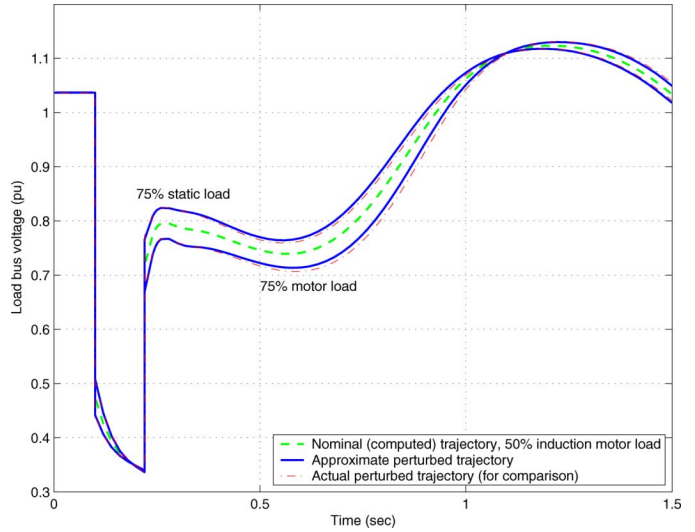
At 0.1 s, a three-phase fault occurred midway along one of the parallel lines between the load and generator buses. The line was tripped at 0.22 s, clearing the fault. The nominal trajectory, shown as a dashed line in Fig. 12, was obtained with $\nu = 0.5$, i.e., equal amounts of motor and voltage-dependent load. Approximate trajectories were then formed for $\Delta\nu = \pm 0.25$. (The positive change gave a load composition of 75% static load, 25% motor load; the negative change gave the reverse percentages.) These approximate trajectories are shown as solid lines. For comparison, the corresponding exact (fully simulated) trajectories are shown as dash-dot lines. The approximations presented in this example are very accurate, even though parameter variation of ± 0.25 is large.

It may be concluded that the effects of diverse load compositions can be assessed for the computational cost of a single simulation.

V. Trajectory Uncertainty

Investigations of power system dynamic behavior typically involve numerous uncertain parameters. The difficulty of quantifying load behavior has previously been discussed. Distributed generation provides another example that is growing in importance. A thorough understanding of the influence of uncertain parameters requires many simulations. However, the computational effort involved in each simulation generally precludes anything more than a cursory examination of parametric dependencies.

Trajectory approximations, given by (31)–(32), overcome the need for repetitive simulation, though at the cost of some loss of accuracy. The affine nature of (31)–(32) allows two straightforward approaches to quantifying the effects of uncertainty: worst-case analysis and probabilistic assessment. Details are provided in the following sections.

A. Worst-Case Analysis

Worst-case analysis builds on an assumption that uncertain parameters are uniformly distributed over a specified range.

Based on that assumption, parameter values at the extremes have the same likelihood of occurrence as any other values within the specified range. Therefore, worst-case (extreme) scenarios cannot be treated as inconsequential and should satisfy dynamic performance criteria.

Uncertainty in numerous parameters gives rise to a uniform distribution over the (convex) orthotope[7]

$$\mathcal{B} = \{\Delta x_0 : \Delta_{\min} \leq \Delta x_0 \leq \Delta_{\max}\} \qquad (39)$$

where Δx_0 describes the deviations from the nominal parameter values, $\Delta_{\min}$ and $\Delta_{\max}$ are vectors of minimum and maximum allowable deviations, respectively, and the inequalities are on an element-by-element basis. The dimension of the orthotope $\mathcal{B}$ matches the number of uncertain parameters. Its vertices are extremes where every element of Δx_0 takes either its maximum or minimum value. Trajectory approximations (31)–(32) describe a time-dependent affine transformation of initial conditions $\Delta x_0 \in \mathcal{B}$, provided the following assumption is satisfied.

Assumption 2: All trajectories emanating from the set $x_0 + \mathcal{B}$ have the same order of events. In other words, grazing does not occur along any of these trajectories.

Under the affine transformations (31)–(32), the orthotope $\mathcal{B}$ is shifted and distorted to form time-dependent parallelotopes[8]

$$\mathcal{P}^\phi(t) = \phi(x_0, t) + \Phi(x_0, t)\mathcal{B} \qquad (40)$$
$$\mathcal{P}^\psi(t) = \psi(x_0, t) + \Psi(x_0, t)\mathcal{B}. \qquad (41)$$

Importantly, the affine transformation maintains convexity [35], with vertices of $\mathcal{B}$ mapping to vertices of $\mathcal{P}^\phi(t)$ and $\mathcal{P}^\psi(t)$. Therefore, (40)–(41) describe the propagation of a convex set through state space.[9] Initial conditions that lie within $x_0 + \mathcal{B}$ give rise to (approximate) trajectories that remain within the time-propagated parallelotopes.

As a consequence of convexity, extremes of behavior can be immediately determined by applying (31)–(32) to just the vertices of $\mathcal{B}$. However, p uncertain parameters result in 2^p vertices. Even approximate propagation of these vertices can become computationally unwieldy. Fortunately, not all vertices need be considered. A reduction process is presented in Section V-C, following an illustration of parallelotope propagation.

B. Example—Parallelotope Propagation

This illustration uses the system described in Section IV-B. The thicker solid trajectory in Fig. 13 shows the angle-frequency phase portrait for the third case considered in Section IV-B, with $\omega(t_0) = 6$ rad/s. An error bound of $-0.1 \leq \Delta\alpha(t_0) \leq 0.1$ was chosen for the initial value of the angle α, and $-1 \leq \Delta\omega(t_0) \leq 1$ for frequency ω. Also, it was assumed the generator inertia could be in error by $-0.075 \leq \Delta H/H \leq 0.075$. This initial

---

[7]An orthotope is a high-dimensional generalization of a rectangle [33].

[8]A parallelotope is a high-dimensional generalization of a parallelogram [33]. Parallel faces remain parallel under the affine transformation, but orthogonality of adjacent faces is lost. Full details can be found in [34].

[9]Similar sensitivity-based worst-case concepts have been explored previously, in the context of component tolerance effects in electronic circuits [36]–[38]. In that application, though, interest focused on steady-state behavior, with sensitivities derived from equilibrium conditions.
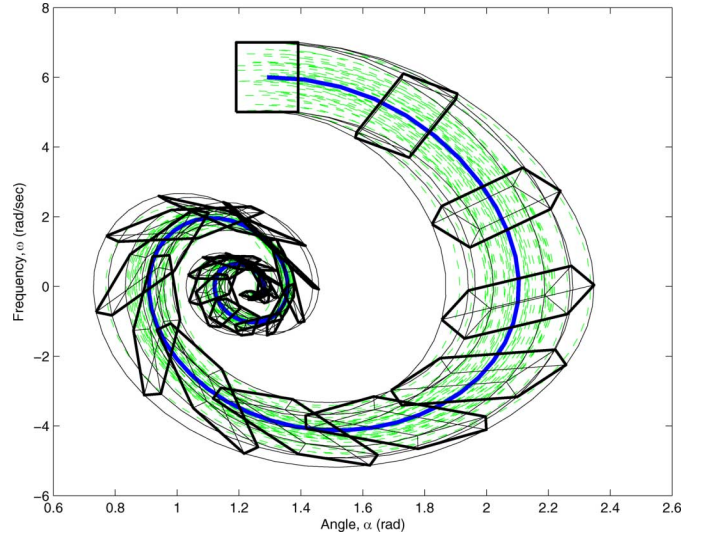

Fig. 13. Phase portrait view of parallelotope propagation.

error orthotope $\mathcal{B}$ is projected onto the $\alpha - \omega$ plane as the rectangle symmetrically surrounding the initial point of the nominal trajectory.

The figure shows the propagation of $\mathcal{B}$ according to (40)–(41). The approximate trajectories emanating from the vertices of $\mathcal{B}$ are shown as thinner solid lines, while the distortion of $\mathcal{B}$ along the trajectory is shown as the sequence of parallelotopes. The projection onto the $\alpha - \omega$ plane flattens these parallelotopes. Their outline, or convex hull [35], is shown as a darker line.

Forty sets of initial conditions were randomly selected from $x_0 + \mathcal{B}$, assuming a uniform distribution. The true (simulated) trajectories arising from those initial conditions are shown as lighter dashed lines. It can be seen that these trajectories lie (almost completely) within the region covered by the propagated parallelotopes, the outline of which is given by the approximate trajectories arising from the vertices of $\mathcal{B}$.

C. Worst-Case Vertices

Generally, only a subset of states is of interest in assessing dynamic performance. For example, Fig. 13 shows only angle and frequency states, even though the full state space is 12-dimensional. This projection to a lower dimensional space maintains convexity. The vertices of the resulting lower dimensional polytopes are a subset of the vertices of the corresponding higher dimensional parallelotopes. This can be observed in Fig. 13.

At any time $t \geq t_0$, a particular dynamic or algebraic state $\zeta(t)$ will lie (approximately) in an interval $\overline{\mathcal{P}}(t)$ that is the projection of $\mathcal{P}^\phi$ or $\mathcal{P}^\psi$, as appropriate. The upper and lower bounds on $\overline{\mathcal{P}}(t)$ correspond to two of the vertices of $\mathcal{B}$. Those vertices describe the parameter deviations that induce worst-case behavior in the chosen state ζ at time t.

Even though $\mathcal{B}$ may have a large number of vertices, locating the two that give the upper and lower bounds is straightforward. Let $S(t)$ be the row of $\Phi(x_0, t)$ or $\Psi(x_0, t)$, as appropriate, corresponding to the quantity of interest $\zeta(t)$. From (31)–(32), the deviation $\Delta\zeta$ resulting from a perturbation Δx_0 can be written

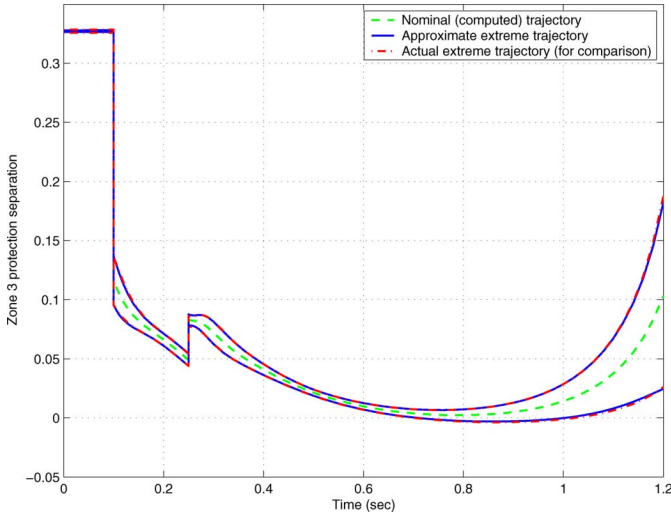$$\Delta\zeta(t) \approx S(t)\Delta x_0. \qquad (42)$$

Fig. 14. Zone 3 protection on line 23–24, worst-case bounds for $0.3 \leq \nu_{23}, \nu_{24} \leq 0.7$.

It follows that the extremes in $\Delta\zeta(t)$, i.e., the upper and lower bounds on the interval $\overline{\mathcal{P}}(t)$, can be determined directly from the signs of the elements of $S(t)$. The upper bound is obtained by setting the ith element of Δx_0 according to

$$[\Delta x_0]_i = \begin{cases} \Delta_{\max}, & \text{if } S_i(t) > 0 \\ \Delta_{\min}, & \text{if } S_i(t) < 0 \end{cases} \qquad (43)$$

where S_i refers to the ith element of row vector S. Likewise, the lower bound is given by

$$[\Delta x_0]_i = \begin{cases} \Delta_{\min}, & \text{if } S_i(t) > 0 \\ \Delta_{\max}, & \text{if } S_i(t) < 0. \end{cases} \qquad (44)$$

The critical values of uncertain parameters are revealed directly by (43) and (44). If behavior is acceptable for the bounding trajectories, then it will be acceptable for any choice of parameters over the range of uncertainty. In other words, every point within $x_0 + \mathcal{B}$ gives rise to behavior that lies (approximately) within the trajectories that bound $\overline{\mathcal{P}}(t)$.

The vertices associated with the bounds on the uncertainty interval $\overline{\mathcal{P}}(t)$ may change with time. However, the procedure outlined above allows efficient tracking of the bounding vertices. Generally, worst-case analysis focuses on specific portions of the trajectory, rather than the complete time response. The bounds need only be computed over the time periods of interest.

D. Example—Worst-Case Analysis

The IEEE 39-bus system of Fig. 1 will be used to illustrate worst-case analysis in a more realistic system. The disturbance scenario for this case involves a solid three-phase fault on line 16–21, at the bus 21 end. The fault was cleared after 0.15 s by tripping the faulted line. That left buses 21 and 23, and generators 6 and 7, radially fed over line 23–24.

An aim of this example is to highlight the importance of accounting for uncertainty when assessing protection operation. Unfortunately, the 39-bus system is not naturally susceptible to

cascading protection trips.[10] Therefore, to enhance the illustration, the impedance of line 23–24 has been scaled up by a factor of 1.5.

The loads at buses 23 and 24 were modeled according to (1), with ν_{23} and ν_{24} both nominally set to 0.5. In other words, both loads were composed of 50% static voltage-dependent load and 50% induction motor load. The static load component was modeled as constant admittance, while the induction motor component used parameter values from [16, p. 305], with appropriate per unit scaling.

An uncertainty of ± 0.2 was assumed in both load composition parameters, so that

$$0.3 \leq \nu_{23}, \nu_{24} \leq 0.7. \qquad (45)$$

Worst-case analysis was used to explore bounds on behavior and, in particular, to determine whether this uncertainty could affect conclusions regarding protection operation.

The example focuses on zone 3 protection at the bus 23 end of line 23–24. Fig. 14 shows the separation between the zone 3 mho characteristic [24] and the apparent impedance seen from bus 23. (This separation goes negative when the apparent impedance enters the mho characteristic.) The dashed line was obtained using the nominal set of load parameters. It remains above zero, suggesting the zone 3 characteristic is not entered. Based on this nominal trajectory, sensitivities indicated that over the time frame of interest, where the trip signal approached zero, worst behavior (lowest dip) occurred for load indexes $\nu_{23} = 0.7$ and $\nu_{24} = 0.3$. Best behavior (least dip) occurred for $\nu_{23} = 0.3$ and $\nu_{24} = 0.7$. The corresponding approximate (sensitivity derived) bounds on behavior are shown as solid lines in Fig. 14. The true (simulated) bounds are shown as dash-dot lines. The sensitivity-based predictions are very accurate over this crucial time period. Every selection of ν_{23} and ν_{24} from the range (45) results in a trajectory that lies within the bounds shown in Fig. 14. Notice that the lower bound passes below zero, indicating the possibility of a zone 3 trip.

This example was extended to incorporate load index uncertainty

$$1.8 \leq \eta_p, \eta_q \leq 2.2 \qquad (46)$$

for all loads throughout the system, together with the load uncertainty expressed by (45). Fig. 15 indicates that this extra uncertainty has little effect on the worst-case bounds before about 0.8 s. Beyond that time, though, the bounds grow quite considerably. (For comparison, the bounds from Fig. 14 are shown as dotted lines in Fig. 15.) Even though uncertainty in a large number of parameters leads to wide bounds, the approximate bounds are still very accurate.[11]

As mentioned previously, the nominal trajectory does not dip below zero, implying zone 3 protection is not a concern. However, the lower bound in Fig. 15 remains below zero for a considerable time, indicating a nontrivial probability of a zone 3

---

[10]Many real power systems are susceptible to cascading protection operation. However, availability of data for those systems is rather limited.

[11]Uncertainty in other parameters, including those describing the induction motor loads, was also considered. Qualitatively similar outcomes were obtained, namely, widening of the uncertainty bounds, with good accuracy maintained.
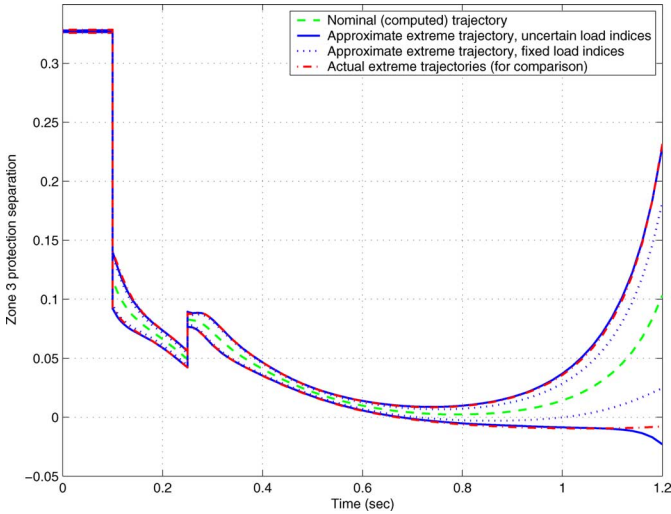
Fig. 15. Zone 3 protection on line 23–24, worst-case bounds for $1.8 \leq \eta_p, \eta_q \leq 2.2$ and $0.3 \leq \nu_{23}, \nu_{24} \leq 0.7$.
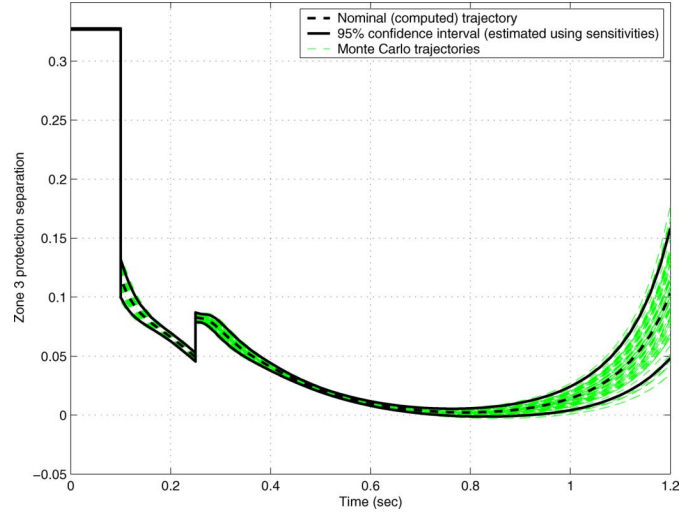

Fig. 16. Zone 3 protection on line 23–24, 95% confidence interval bounds for $E[\nu_{23}] = E[\nu_{24}] = 0.5$, $\text{Var}[\nu_{23}] = \text{Var}[\nu_{24}] = 0.01$.

trip. This example highlights the importance of considering uncertainty when assessing protection response.

In both Figs. 14 and 15, the worst-case bounds exhibit rapid growth over the period 1 to 1.2 s. The explanation lies in the system stability margin. For the nominal parameter set, the critical clearing time was 0.163 s, compared with the actual clearing time of 0.15 s used throughout the example. With load parameters altered to reflect the worst-case behavior in Fig. 15, the critical clearing time dropped to 0.151 s. The actual clearing time of 0.15 s therefore induced behavior that was almost unstable. As indicated in Section III-D, proximity to instability implies large sensitivity to parameter variations. The rapid growth in the worst-case bounds reflects that sensitivity. Importantly, even though the system is only marginally stable, the trajectory approximations are still accurate.

E. Probabilistic Assessment

Often parameter values are not uniformly distributed over the range of uncertainty but tend more toward a normal distribution. Under those conditions, worst-case analysis gives a conservative view of parametric influences. Less conservatism is achieved with probabilistic assessment.

A probabilistic approach to assessing the influence of uncertainty assumes x_0 is a random vector[12] with mean μ and covariance matrix Σ. It follows that deviations

$$\Delta x_0 = x_0 - \mu \qquad (47)$$

have zero mean and covariance Σ. Let the mean μ describe the initial conditions for the nominal flow and trajectory sensitivities, i.e., μ establishes the nominal parameter set. Then from (42), and basic statistical properties [39], perturbations $\Delta\zeta(t)$ in any particular quantity of interest ζ, will have mean

$$E[\Delta\zeta(t)] = S(t) E[\Delta x_0] = 0 \qquad (48)$$

[12]Certain elements of x_0 will be known exactly. For such elements, the corresponding row and column of Σ are zero.

and variance

$$\text{Var}[\Delta\zeta(t)] = S(t) \Sigma S(t)^T \qquad (49)$$

where $S(t)$ is the row of $\Phi(\mu, t)$ or $\Psi(\mu, t)$ corresponding to ζ. Furthermore, if the elements of random vector Δx_0 are statistically independent, then Σ becomes a diagonal matrix with $\sigma_1^2 \ldots \sigma_n^2$ along the diagonal, and (49) reduces to

$$\text{Var}[\Delta\zeta(t)] = \sum_{i=1}^{n} S_i(t)^2 \sigma_i^2. \qquad (50)$$

F. Example—Probabilistic Assessment

This example uses the same system and fault scenario as in Section V-D. In this case, however, the uncertain load composition variables ν_{23} and ν_{24} are both normally distributed, with mean (nominal) values $E[\nu_{23}] = E[\nu_{24}] = 0.5$. It is assumed the random perturbations in these variables are independent and have variances $\text{Var}[\nu_{23}] = \text{Var}[\nu_{24}] = 0.01$. The parameter range (45) therefore corresponds to ± 2 standard deviations. The probability of parameters lying within that range is 95.45%.

The parameter of interest ζ in this case, as in the example of Section V-D, is the zone 3 protection signal. Fig. 16 shows the response of that signal, with nominal behavior indicated by the thick dashed line. (This nominal response corresponds exactly with the nominal trajectory in Fig. 14.) Equation (50) was used to determine the time varying (approximate) variance of $\zeta(t)$, given that $\sigma^2 = 0.01$ for both uncertain parameters. The 95% confidence interval obtained using this variance is denoted in Fig. 16 by solid lines. For comparison, a Monte Carlo process was used to generate 100 pairs of random variables (ν_{23}, ν_{24}), with the corresponding trajectories shown in Fig. 16 by lighter dashed lines. It can be seen that the 95% confidence interval captures most of the behavior, though some trajectories lie outside that interval.
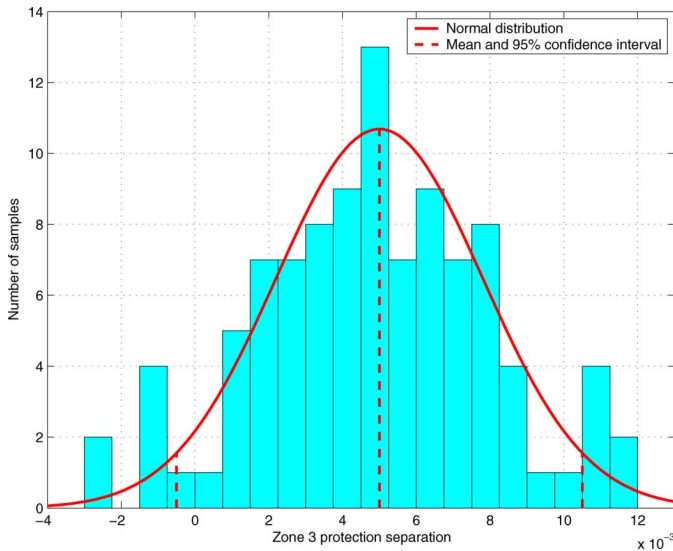
Fig. 17. Zone 3 protection on line 23–24, signal distribution at 0.9 s, $E[\nu_{23}] = E[\nu_{24}] = 0.5$, $\mathrm{Var}[\nu_{23}] = \mathrm{Var}[\nu_{24}] = 0.01$.

TABLE I
COMPARISON OF MONTE CARLO AND SENSITIVITY-BASED STATISTICS

Time	Monte Carlo		Sensitivity	
(sec)	Mean	Std dev	Mean	Std dev
0.8	0.0022	0.0020	0.0023	0.0017
0.9	0.0049	0.0031	0.0050	0.0028
1.0	0.0140	0.0058	0.0141	0.0051

A clearer view of the statistical distribution of trajectories can be obtained by focusing on particular time instants. For example, the histogram of Fig. 17 shows the distribution of random trajectories at $t = 0.9$ s. Overlaying that histogram is the probability density function (pdf) for the normal distribution with mean given by the nominal trajectory and variance calculated from the sensitivity-based approximation (50). Given the relatively small number of samples, the histogram matches the pdf quite closely.

Table I provides a comparison of sensitivity-based statistics with Monte Carlo results, for three time instants. The sensitivity-based mean corresponds to the nominal trajectory, while the standard deviation is the square root of the variance given by (50). It seems the sensitivity-based approximation tends to underestimate the standard deviation slightly. However, the error is insignificant given the relatively small number of samples in the Monte Carlo process.

VI. CONCLUSIONS

Parameters of many power system models can never be known exactly. Composite load models are particularly challenging to parameterize, due to their stochastic nature. (This is also the case for high-penetration distributed generation.) Yet the results of power system simulation studies are routinely used in planning and operating decisions. Therefore, it is important to quantify the errors introduced by parameter uncertainty. This paper provides techniques for (approximately) bounding those errors.

Trajectory sensitivities can be efficiently computed as a by-product of simulating the nominal trajectory. These sensitivities offer a way of ranking the relative influence of parameters. More importantly for this paper, they provide the basis for generating first-order approximations of trajectories that arise from perturbed parameter sets. Dynamic behavior can be expressed in functional form (as the flow) and expanded as a Taylor series. Approximate behavior is obtained by neglecting higher order terms. It is shown in this paper that the error introduced by truncating the expansion is affected by proximity to instability (system stress) and the magnitude of parameter perturbations. As systems become more heavily stressed, perturbation size must decrease to maintain commensurate accuracy. Approximate trajectories are well defined for nonsmooth behavior.

Sensitivity-based trajectory approximations have an affine structure, motivating two straightforward approaches to quantifying the effects of uncertainty: worst-case analysis and probabilistic assessment. Worst-case analysis involves propagating the vertices of an orthotope that describes initial uncertainty. A simple algorithm allows the bounding (worst case) vertices to be efficiently, though approximately, determined. Probabilistic assessment uses trajectory sensitivities to map variances of uncertain parameters to the time-varying variances of states. These variances can be used to establish a confidence interval around the nominal trajectory.

The extra information provided by uncertainty bounds establishes a clearer view of likely system behavior. This is particularly valuable in assessing the likelihood of risks such as cascade-inducing protection operation. Provision of this supplementary information involves straightforward implementation and negligible computational burden.

REFERENCES

[1] R. Craven, T. George, G. Price, P. Wright, and I. Hiskens, "Validation of dynamic modelling methods against power system response to small and large disturbances," in *Proc. CIGRÉ General Session*, Paris, France, Aug. 1994.

[2] J. Hauer, W. Mittelstadt, W. Litzenberger, C. Clemens, D. Hamai, and P. Overholt, Wide Area Measurements for Real-Time Control and Operation of Large Electric Power Systems, DOE Final Rep., 1999.

[3] I. Hiskens, "Nonlinear dynamic model evaluation from disturbance measurements," *IEEE Trans. Power Syst.*, vol. 16, no. 4, pp. 702–710, Nov. 2001.

[4] F. Wu and Y.-K. Tsai, "Probabilistic dynamic security assessment of power systems," *IEEE Trans. Circuits Syst.*, vol. CAS-30, no. 3, pp. 148–159, Mar. 1983.

[5] P. Anderson and A. Bose, "A probabilistic approach to power system stability analysis," *IEEE Trans. Power App. Syst.*, vol. PAS-102, pp. 2430–2439, Aug. 1983.

[6] J. Hockenberry and B. Lesieutre, "Evaluation of uncertainty in dynamic simulation of power system models: The probabilistic collocation method," *IEEE Trans. Power Syst.*, vol. 19, no. 3, pp. 1483–1491, Aug. 2004.

[7] A. Monti, F. Ponci, T. Lovett, A. Smith, and R. Dougal, "Modeling of uncertainty and applications in monitoring and control of power electronics," in *Proc. Amer. Control Conf.*, Portland, OR, Jun. 2005, pp. 2011–2016.

[8] I. Hiskens, M. Pai, and T. Nguyen, "Bounding uncertainty in power system dynamic simulations," in *Proc. IEEE Power Eng. Soc. Winter Meeting*, Singapore, Jan. 2000.

[9] R. Tomović, *Sensitivity Analysis of Dynamic Systems*. New York: McGraw-Hill, 1963.

[10] J. Cruz Jr., *System Sensitivity Analysis*. Stroudsburg, PA: Dowden, Hutchinson and Ross, 1973.

[11] P. Frank, *Introduction to System Sensitivity Theory*. New York: Academic, 1978.
[12] W. Feehery, J. Tolsma, and P. Barton, "Efficient sensitivity analysis of large-scale differential-algebraic systems," *Appl. Numer. Math.*, vol. 25, pp. 41–54, 1997.
[13] I. Hiskens and M. Pai, "Trajectory sensitivity analysis of hybrid systems," *IEEE Trans. Circuits Syst. I, Fundam. Theory Appl.*, vol. 47, no. 2, pp. 204–220, Feb. 2000.
[14] IEEE Task Force Report, "Standard load models for power flow and dynamic performance simulation," *IEEE Trans. Power Syst.*, vol. 10, no. 3, pp. 1302–1313, Aug. 1995.
[15] L. Pereira, D. Kosterev, P. Mackin, D. Davies, J. Undrill, and W. Zhu, "An interim dynamic induction motor model for stability studies in the WSCC," *IEEE Trans. Power Syst.*, vol. 17, no. 4, pp. 1108–1115, Nov. 2002.
[16] P. Kundur, *Power System Stability and Control*. New York: McGraw-Hill, 1994, EPRI Power System Engineering Series.
[17] A. van der Schaft and H. Schumacher, *An Introduction to Hybrid Dynamical Systems*. London, U.K.: Springer-Verlag, 2000.
[18] D. Liberzon, *Switching in Systems and Control*. Boston, MA: Birkhauser, 2003.
[19] M. di Bernardo, H. Chung, and C. Tse, "Guest editorial: Special issue on switching and systems," *IEEE Trans. Circuits Syst. I, Fundam. Theory Appl.*, vol. 50, no. 8, pp. 973–974, Aug. 2003.
[20] R. David and H. Alla, *Petri Nets and Grafecet*. Englewood Cliffs, NJ: Prentice-Hall, 1992.
[21] I. Hiskens, "Power system modeling for inverse problems," *IEEE Trans. Circuits Syst. I, Reg. Papers*, vol. 51, no. 3, pp. 539–551, Mar. 2004.
[22] V. Donde and I. Hiskens, "Dynamic performance assessment: Grazing and related phenomena," *IEEE Trans. Power Syst.*, vol. 20, no. 4, pp. 1967–1975, Nov. 2005.
[23] E. Lee and H. Zheng, "Operational semantics of hybrid systems," in *Hybrid Systems: Computation and Control*, M. Morari and L. Thiele, Eds. New York: Springer, 2005, vol. 3414, Lecture Notes in Computer Science, pp. 25–53.
[24] J. Blackburn, *Protective Relaying Principles and Applications*, 2nd ed. New York: Marcel Dekker, 1998.
[25] C. Fox, *An Introduction to the Calculus of Variations*. New York: Dover, 1988.
[26] A. Bryson and Y. Ho, *Applied Optimal Control*. New York: Taylor & Francis, 1975.
[27] S. Li, L. Petzold, and W. Zhu, "Sensitivity analysis of differential-algebraic equations: A comparison of methods on a special problem," *Appl. Numer. Math.*, vol. 32, no. 8, pp. 161–174, 2000.
[28] P. Sauer and M. Pai, *Power System Dynamics and Stability*. Upper Saddle River, NJ: Prentice-Hall, 1998.
[29] *IEEE Recommended Practice for Excitation System Models for Power System Stability Studies*, IEEE Std. 421.5-1992, 1992.
[30] M. Pai, *Energy Function Analysis for Power System Stability*. Norwell, MA: Kluwer, 1989.
[31] I. Hiskens, M. Pai, and T. Nguyen, "Dynamic contingency analysis studies for inter-area transfers," in *Proc. 13th Power Systems Computation Conf.*, Trondheim, Norway, Jun. 1999.
[32] T. Nguyen, M. Pai, and I. Hiskens, "Sensitivity approaches for direct computation of critical parameters in a power system," *Int. J. Elect. Power Energy Syst.*, vol. 24, pp. 337–343, 2002.
[33] H. Coxeter, *Regular Polytopes*, 3rd ed. New York: Dover, 1973.
[34] A. Brøndsted, *An Introduction to Convex Polytopes*. New York: Springer-Verlag, 1983.
[35] R. Rockfellar, *Convex Analysis*. Princeton, NJ: Princeton Univ. Press, 1970.
[36] J. Bandler, P. Liu, and J. Chen, "Worst-case network tolerance optimization," *IEEE Trans. Microw. Theory Tech.*, vol. MTT-23, pp. 630–641, Aug. 1975.
[37] R. Spence and R. Soin, *Tolerance Design of Electronic Circuits*. Reading, PA: Addison-Wesley, 1988.
[38] M. Tian and C.-J. Shi, "Worst case tolerance analysis of linear analog circuits using sensitivity bands," *IEEE Trans. Circuits Syst. I*, vol. 47, no. 8, pp. 1138–1145, Aug. 2000.
[39] E. Kreyszig, *Introductory Mathematical Statistics*. New York: Wiley, 1970.

Ian A. Hiskens (S'77–M'80–SM'96–F'06) is a Professor of electrical and computer engineering at the University of Wisconsin-Madison. He received the B.Eng. degree in electrical engineering and B.App.Sc. degree in mathematics from the Capricornia Institute of Advanced Education, Rockhampton, Australia, in 1980 and 1983, respectively, and the Ph.D. degree from the University of Newcastle, Newcastle, Australia, in 1991.

He has held prior appointments with the Queensland Electricity Supply Industry, Australia, from 1980 to 1992, the University of Newcastle from 1992 to 1999, and the University of Illinois at Urbana-Champaign from 1999 to 2002. His major research interests lie in the area of power system analysis, in particular system dynamics, security, and numerical techniques. Other research interests include nonlinear and hybrid systems, and control.

Dr. Hiskens was an Associate Editor of the IEEE Transactions on Circuits and Systems I from 2002 to 2005 and is currently Treasurer of the IEEE Systems Council.

Jassim Alseddiqui (S'02) received the B.Sc. degree in electrical engineering (with distinction) from the University of Wisconsin-Madison in 2004 and the M.S. degree in electrical engineering from Cornell University, Ithaca, NY, in 2005.

He is an Instructor at the Petroleum Institute, Abu Dhabi, United Arab Emirates, and an Electrical Engineer Trainee at Abu Dhabi Gas Industries Ltd. (GASCO). His research interests are nonlinear systems, power systems, power system planning, nonlinear optimization, global optimization, and engineering economics.

Mr. Alseddiqui is a member of Eta Kappa Nu, Tau Beta Pi, Golden Key International, and the Burrill Business Association. He is also the founder and the current president of the Emirates Association for Innovation and Technology.